Polyhedron 129 (2017) 214–221

Contents lists available at ScienceDirect

Polyhedron

journal homepage: www.elsevier.com/locate/poly

Propyl gallate metal complexes: Circular dichroism, BSA-binding, antioxidant and cytotoxic activity

Murilo Massoni [a], Juan C. Tenorio Clavijo [b], Legna Colina-Vegas [c], Wilmer Villarreal [c], Julia S.M. Dias [a], Guilherme A.F. da Silva [d], Marisa Ionta [d], Marisi Soares [a], Javier Ellena [b], Antônio C. Dorigueto [a], Marília I.F. Barbosa [a,*], Alzir A. Batista [c,*]

[a] Instituto de Química, Universidade Federal de Alfenas, CEP 37130-000, Alfenas, MG, Brazil
[b] Instituto de Física de São Carlos, Universidade de São Paulo, CP 369, CEP 13560-970 São Carlos, SP, Brazil
[c] Departamento de Química, Universidade Federal de São Carlos, CP 676, CEP 13565-905 São Carlos, SP, Brazil
[d] Instituto de Ciências Biomédicas, Universidade Federal de Alfenas, CEP: 37130-000, Alfenas, MG, Brazil

ARTICLE INFO

Article history:
Received 17 February 2017
Accepted 28 March 2017
Available online 5 April 2017

Keywords:
Propyl gallate complexes
Anticancer activity
BSA-binding experiments
Antioxidant activity
Platinum(II) and Ruthenium (II) complexes

ABSTRACT

Herein syntheses and characterization of the complexes $[Pt(PG)(PPh_3)_2]$ (**1**) and $[Ru(PG)(dppm)_2]$ (**2**), where PG (propyl gallate) = propyl 3,4,5-trihydroxybenzoate, PPh_3 = triphenylphosphine and dppm = 1,1-bis(diphenylphosphino) methane, are described. The structure of the complex $[Pt(PG)(PPh_3)_2]$ was elucidated by X-ray diffraction. The cytotoxicity of the complexes against four tumor cell lines, lung carcinoma (A549), breast carcinoma (MCF-7), hepatocellular carcinoma (HepG2), glioblastoma (U251MG), and a normal fibroblast (CCD-1059Sk) were evaluated. The selectivity index values showed that complex (**2**) is more potent and selective than the free propyl gallate molecule and complex (**1**). Furthermore, complex (**2**) is a slightly higher active against the tumor cells MCF-7 and HepG2 than the cisplatin. In addition, BSA-binding experiments and antioxidant activity of the complexes were evaluated. The interactions of the complexes with the BSA showed negative ΔH and ΔS values, leading to van der Waals force or hydrogen bond formation between the complexes and the biomolecule. Furthermore, the negative ΔG values reveal that the interaction process of complex/BSA is spontaneous. It was observed that the $[Pt(PG)(PPh_3)_2]$ complex has an inhibitory effect against free radicals, whereas $[Ru(PG)(dppm)_2]$ was not active. Circular dichroism showed that the free ligand and the complexes are unable to modify the DNA secondary structure of this biomolecule.

1. Introduction

Cancer is a leading cause of death worldwide, accounting for 8.2 million deaths in 2014. Lung, liver, stomach, colorectal and breast cancers cause many cancer deaths each year [1]. Studying and developing effective drugs for cancer treatment with non-genotoxic effects is extremely important, considering that different types of new mutations and genetic abnormalities are critical in promoting tumor resistance to current therapies [2–6].

Metal complexes have been fundamental in the development of modern chemotherapy. Since the discovery of the antitumor properties of cisplatin, many studies have focused on obtaining complexes with other metals, which could have advantages compared to platinum compounds, such as changes in the affinity of the binder for the metal and substitution kinetics, changes in their oxidation state, use in photodynamic therapy and with low or no toxic effect [3,4].

Thus, growing interest in metallotherapeutic drugs has motivated new designs for anticancer metal compounds, and various results on this subject have been published and many of them are reported in recent articles or reviews [7–10]. In fact, the aim of this kind of research is to design and develop novel antitumoral drugs with better efficiency, lower toxicity and less undesirable side effects than the current drugs that are on the market [8,9]. Taking this into account, it is crucial to conduct research on new active compounds with antitumor properties.

Propyl gallate presents antitumor, antimicrobial, antiviral, as well as a potent antioxidant activity, acting as a sequester of reactive oxygen species [11]. This molecule or its derivatives also present *in vitro* and *in vivo* activity against various tumor cell lines, including cell lines of leukemia, melanoma, lung and breast cancer [12–14]. Additionally, arylspiroborate salts derived from

* Corresponding authors.
E-mail addresses: mariliaifrazaob@gmail.com (M.I.F. Barbosa), daab@ufscar.br (A.A. Batista).

http://dx.doi.org/10.1016/j.poly.2017.03.055
0277-5387/

pyrogallol, gallic acid and propyl gallate were described as having a cytotoxic effect on renal cell carcinoma [15,16]. Also, the synergistic interaction of PG/Cu(II) demonstrate DNA strand break induction and enhanced cytotoxicity of propyl gallate [17].

For this study, the propyl gallate (Fig. 1) was isolated from *Caesalpinia* var. *peltophodoires* and was used here for the coordination with metallic ions of platinum and ruthenium, aiming to obtain complexes with good antitumor activities.

The chemical reactivity of the propyl gallate molecule with precursors such as $[PtCl_2(PPh_3)_2]$ and $[RuCl_2(dppm)_2]$ enabled us to synthesize complexes with formulae $[Pt(PG)(PPh_3)_2]$ (**1**) and $[Ru(PG)(dppm)_2]$ (**2**), where PG = propyl gallate, PPh_3 = triphenylphospine and dppm = 1,1-bis(diphenylphosphino)methane. Therefore, this study describes the synthesis, characterization, anticancer activities, BSA-binding, circular dichroism and oxidant activity of novel gallate complexes.

2. Experimental

2.1. Materials for synthesis

Solvents were purified by standard methods. All chemicals used were of reagent grade or comparable purity. $RuCl_3{\cdot}3H_2O$, $[PtCl_2(PPh_3)_2]$ and the ligands 1,1-bis(diphenylphosphino) methane, triphenylphosphine and triethylamine (Et_3N), were used as received from Aldrich. The propyl gallate was obtained from crude extract of roots of *Caesalpinia pluviosa var. peltophoroides* after being treated with 20.0 g of ethyl acetate fraction, under chromatography. From those, the ones numbered from 1 to 10 (420 mg) were purified by using silica and Sephadex and 31.0 mg of a white crystal presenting melting temperature around 146 °C was found. The final product was subsequently confirmed by NMR ^1H, ^{13}C and DEPT experiments (see Supplementary material, Figs. S1–S3).

2.2. Instrumentation

Elemental analyses were performed in a Fisons EA 1108 model (Thermo Scientific). The IR spectra of the powder complexes were recorded using CsI pellets in the 4000–200 cm^{-1} region in a Bomen–Michelson FT MB-102 instrument. The UV–Vis spectra of the complex were recorded in CH_2Cl_2 solution, in a Hewlett Packard diode array – 8452A. Cyclic voltammetry (CV) experiments of the complexes, in solution, were promoted in an electrochemical analyzer BAS model 100B. These experiments were carried out at room temperature in CH_2Cl_2 containing 0.10 mol L^{-1} $Bu_4N^+ClO_4^-$ (TBAP) (FlukaPurum) as a support electrolyte, using a one-compartment cell with both working and auxiliary electrodes, which were stationary Pt foils, while the reference electrode was Ag/AgCl, 0.10 M TBAP in CH_2Cl_2. Under these conditions, the ferrocene is oxidized at 0.43 V (Fc^+/Fc). All NMR experiments were run on BRUKER, DRX400 MHz equipment, in a BBO 5 mm probe, at 298 K and TMS for internal reference. CH_2Cl_2 was used as solvent for $^{31}P\{^1H\}$ NMR. Conductivity measurements of acetone solutions (1.0 mmol L^{-1}) of the complexes were carried out using a Meter Lab CDM2300 conductivity meter with a cell of constant 0.089 cm^{-1}.

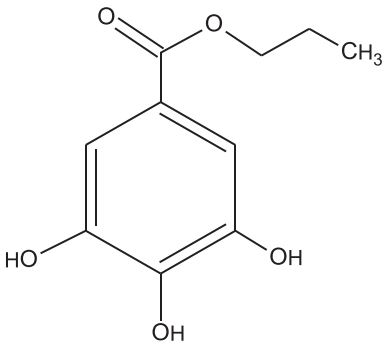

Fig. 1. Structure of the propyl gallate molecule.

2.3. X-ray crystallography

Yellow single crystals of complex **1** were grown by slow evaporation of a dichloromethane/methanol solution. X-ray diffraction experiments were carried out using a suitable crystal mounted on glass fiber and positioned on the goniometer head. Intensity data were measured with the crystal at room temperature on an Enraf–Nonius Kappa-CCD diffractometer with graphite monochromated Mo Kα radiation (λ = 0.71073 Å). The cell refinements were performed using the Collect and Scalepack software [18] and the final cell parameters were obtained from all reflections. Data reduction was carried out using the Denzo-SMN and Scalepack software [19]. The structures were solved by the Direct method using SHELXS-2013 and refined using the software [20]. A GAUSSIAN method was used for the absorption corrections [20]. Non-hydrogen atoms were refined anisotropically (excepted to the disordered C91A and C92A atoms) and hydrogen atoms were fixed at calculated positions and refined using a riding mode. The constrained positions and fixed isotropic thermal parameters for C–H hydrogen atoms were the bond lengths of 0.93, 0.97 and 0.96 Å for C^2_{sp}–H (aromatic rings) and C^3_{sp}–H (methylene and methyl groups), respectively, considering $U_{iso}(H) = 1.2\,U_{eq}(C)$ and $U_{iso}(H) = 1.5U_{eq}(C)$ for methyl hydrogens. The O–H hydrogen atoms of hydroxyl groups were the bond lengths of 0.82 Å with $U_{iso}(H) = 1.5U_{eq}(O)$. Positional disorder was observed in the C91A–C92A atoms of the propyl chain of the gallate ligand to conformer A, which can be reliably modeled. In this case, the disorder was refined over two site occupancy factors (SOF) with 0.4:0.6 of occupancy for C91A:C92A on the propyl chain. Tables were generated by WinGX [21] and the structure representations by ORTEP-3 [22] and MERCURY [23]. The main crystal data collections and structure refinement parameters for (**1**) are summarized in Table 1.

2.4. Synthesis

2.4.1. *[Pt(PG)(PPh$_3$)$_2$]. (**1**)*

Complex **1** was prepared by adding 0.027 g (1.2×10^{-4} mol) of propyl gallate in 20 mL of methanol previously degassed, with the same equivalent of triethylamine (Et_3N) and then 0.084 g (1.1×10^{-4} mol) of the precursor *cis*-$[PtCl_2(PPh_3)_2]$ [24] was added. The reaction mixture was refluxed and stirred for about 24 h under argon atmosphere. The final yellow solution was concentrated to ca. 2 mL and 10 mL of water was added in order to obtain a yellow precipitate. The solid was filtered off, well rinsed with water and diethyl ether and dried in vacuum. Yield: 68.2 mg (67%). *Anal.* Calc. for $C_{46}H_{40}O_5P_2Pt{\cdot}2H_2O$: exp. (calc) C 57.48 (57.20); H 4.97 (4.59). $^{31}P\{^1H\}$ NMR: δ (ppm) 10.8 (d) and 7.7 (d), $^2J_{pp}$ = 32.2 Hz. UV–Vis (CH_2Cl_2): λ nm (ε/L mol^{-1} cm^{-1}) 238 and 303 (shoulder), 332 (3.2×10^3) and molar conductivity, in acetone, 1.90 S cm^2 mol^{-1}.

2.4.2. *[Ru(PG)(dppm)$_2$] (**2**)*

Complex **2** was prepared by adding 0.055 g (2.5×10^{-3} mol) of propyl gallate in 10 mL of CH_2Cl_2, with the same equivalent of Et_3N and then, 0.100 g of the precursor *cis*-$[RuCl_2(dppm)_2]$ [25] (1.6×10^{-3} mol) were added. The reaction mixture was stirred for 24 h under argon atmosphere. The final dark green solution was concentrated to ca. 2 mL and 10 mL of diethyl ether was added

Table 1
Crystal data and structure refinement for complex $[Pt(PG)_2(PPh_3)_2]$.

Empirical formula	$C_{46}H_{40}O_5P_2Pt_1$
Formula weight	929.80
T (K)	293(2)
λ (Å)	0.71073
Crystal system	triclinic
Space group	$P\bar{1}$
Unit cell dimensions	
a (Å)	11.135
b (Å)	13.639
c (Å)	27.953(1)
α (°)	102.532(1)
β (°)	93.363(1)
γ (°)	97.700(2)
V (Å^3)	4089.8(2)
Z, Z'	4, 2
D_{calc} (mg/m3)	1.510
Absorption coefficient (mm^{-1})	3.554
$F(000)$	1856
Crystal size (mm)	0.354 × 0.150 × 0.064
Theta range for data collection	3.006–25.705°
Index ranges	$-12 \le h \le 13$, $-16 \le k \le 16$, $-33 \le l \le 33$
Reflections collected	35956
Independent reflections	15229 [R_{int} = 0.136]
Completeness to theta = 25.242°	98.6%
Refinement method	Full-matrix least-squares on F^2
Data/restraints/parameters	15229/0/972
Goodness-of-fit (GOF) on F^2	0.991
Final R indices [I > 2sigma(I)]	R_1 = 0.0480, wR_2 = 0.0966
R indices (all data)	R_1 = 0.0954, wR_2 = 0.1158
Largest diff. peak and hole (e Å^{-3})	1.081 and −1.081

in order to obtain a green precipitate. The solid was filtered off, well rinsed with diethyl ether and dried in vacuum. Yield: 0.103 g (83%). *Anal.* Calc. for $C_{60}H_{54}O_5P_4Ru$: exp. (calc) C 66.01 (66.72); H 4.97 (5.04). $^{31}P\{^1H\}$ NMR: δ (ppm) 10.0 (t) and −18.9 (t), $^2J_{pp}$ = 39.6 Hz. UV–Vis (CH_2Cl_2): λ/nm (ε/M^{-1} L cm^{-1}) 246 (1.9×10^3), 280 (2.9×10^3) and molar conductivity, in acetone, 3.12 S cm^2 mol^{-1}.

2.5. Biological experiments

2.5.1. Cell lines and treatment schedule

Cell lines derived from human cancer were used in this study: A549 (lung carcinoma), MCF-7 (breast carcinoma), HepG2 (hepatocellular carcinoma), fibroblast (CCD-1059Sk) and U251MG (glioblastoma). The cell cultures were maintained in DMEM (Dulbecco's Modified Eagle's Medium, Sigma, CA, USA) supplemented with 10% fetal bovine serum (Vitrocell, Campinas, Brazil). Cells were grown in a 37 °C humidified incubator containing 5% CO_2. Complexes were solubilized in DMSO immediately before use and an amount of DMSO in the culture medium did not exceed 0.5% (v/v). Cells were seeded into 96-wells plate and after attachment (24 h), the cultures were treated with different compounds for 48 h.

2.5.2. Cell viability analysis

Cell viability was measured by MTS (3-(4,5-dimethylthiazol-2-yl)-5-(3-carboxymethoxyphenyl)-2-(4-sulfophenyl)-2H-tetrazolium) assay using CellTiter 96® Aqueous Non-Radiative Cell Proliferation assay (Promega) according to the manufacturer's instructions. The MTS tetrazolium compound is bioreduced by metabolically active cells into a colored formazan product which absorbs light at 490 nm. The viable cell rate is directly proportional to the amount of formazan produced by dehydrogenase enzymes. Experiments were conducted in triplicate wells and repeated twice. Data are presented as the mean ± standard deviation (SD). The IC_{50} value was determined from non-linear regression using GraphPad Prism® (GraphPad Software, Inc., San Diego, CA, USA).

2.6. BSA fluorescence

Fluorescence spectroscopy is an effective method to explore the interactions between small molecules and BSA. The fluorescence of BSA comes from its tryptophan, tyrosine and phenylalanine residues; the latter two contributing to its fluorescence to only a minor extent [26]. The protein interaction was examined in 96-well plates used for fluorescence assays. BSA (~2.5 μM) was prepared by dissolving the protein in Tris–HCl and the complexes were dissolved in sterile DMSO. For fluorescence measurements, the BSA concentration in buffer Tris–HCl was kept constant in all samples, while the complex concentration was increased from 100 to 0.78 μM, and quenching of the emission intensity of the BSA's tryptophan residues at 344 nm (excitation wavelength 295 nm) was monitored at different temperatures (295 and 310 K).

2.7. Circular dichroism experiments

CD spectra were recorded on a spectropolarimeter JASCO J720 between 600 and 200 nm in a continuous scanning mode (200 nm/min). The final data are expressed in molar ellipticity (millidegrees). All of the CD spectra were generated and represented averages of three scans. Stock solutions (2.0 mM) of each complex were freshly prepared in DMSO prior to use. An appropriate volume of each solution was added to the samples of a freshly prepared solution of CT-DNA (100 μM) in a Tris–HCl buffer to achieve molar ratios ranging from 0.03 to 0.50 drug/DNA. The samples were incubated at 37 °C for 18 h.

2.8. Free radical scavenging activity by 1-diphenyl-2-picrylhydrazyl (DPPH) assay

The antioxidant activity of the novel complexes was determined by their ability to scavenge the stable radical DPPH·. The measurement of the DPPH radical scavenging activity was performed according to the methodology described by Brand-Williams et al. [27]. The samples were reacted with DPPH in a methanol solution (0.04 mg/mL) and for absorption measurements, the DPPH concentration was kept constant, while the compound concentration was increased from 1.56 to 200 μM. The experiments were performed in triplicate in an opaque 96-well microplate. Furthermore, 180 μL of DPPH solution and 10 μL of the compound dissolved in DMSO was added to each well and the control contained 180 μL of DPPH and 10 μL of DMSO. For the sake of comparison, gallic acid (GA) was used as a standard solution as GA has demonstrated to be a strong antioxidant activity in many studies [28]. When DPPH reacts with an antioxidant compound, which can donate hydrogen, it is reduced. The changes in color (from deep violet to light yellow) were read at 520 nm at different times (3, 9, 20 and 30 min) at 25 °C using a Synergy H1 Multi-Mode Reader (BioTek). The scavenging activity percentage (AA%) was determined: $[(A_0 - A_i)/A_0] \times 100$, where A_i is the absorbance in the presence of the tested compound and A_0 is the absorbance in the absence of the tested compound. The antioxidant activity was expressed by the IC_{50} value (concentration of test compound that inhibits the formation of free radicals by 50%), which was calculated from the regression curves where: *x-axis* was the log concentration of the tested compound (in μM) and the *y-axis* was the percentage of inhibition of the tested compounds.

3. Results and discussion

The reaction of propyl gallate with the precursors *cis*-[$RuCl_2(dppm)_2$] and *cis*-[$PtCl_2(PPh_3)_2$ resulted in products **1** and **2**, respectively, by chlorido exchange. In both complexes obtained, the propyl gallate molecule acts as a bidentate and dianionic species, coordinating with the ruthenium and platinum atoms through its *ortho* oxygens (O1, O2 – Fig. 2). Similar behavior was observed for the gallate group when it was coordinated to Fe (II), Fe(III) and Cu(II) ions [29,30].

The elemental analyses data agree well with the proposed formulations for the obtained complexes. The molar conductance values, measured in acetone at room temperature are 1.9 and 3.2 S cm^2 mol^{-1} for the platinum and ruthenium complexes, respectively, revealing no electrolytic nature of these complexes.

The $^{31}P\{^1H\}$ NMR experiment showed two doublets for compound **1** and two triplet resonance signals for compound **2**, indicating the presence of two non-equivalent phosphorus atoms in both complexes. For compound **1**, ^{31}P-^{195}Pt coupling was observed with J = 3120.23 and 3485.81 Hz (see Supplementary material, Figs. S4–S5) for the two chemical distinct phosphorus atoms.

Cyclic voltammetry experiment for **2** was carried out in CH_2Cl_2 solutions. A quasi-reversible process was observed at 1.31 V, respectively, corresponding to a one-electron Ru^{II}/Ru^{III} redox process. As expected, the $E_{1/2}$ values found for the new complexes were considerably more anodic than those observed for the precursor, *cis*-[$RuCl_2(dppm)_2$] (0.89 V), indicating a more stabilized ruthenium center in the new complex, showing that the chlorido is a better donor atom than the oxygen atom from the galate ligand (see Supplementary material, Fig. S6).

The electronic spectra of compounds **1** and **2** showed bands in the UV region, assigned as intra-ligand transitions by means of comparison with the free ligands (dppm, PPh_3 and PG). One band observed in the visible region results from a metal-to-ligand charge transfer transition, probably involving both the PG and the phosphine ligands (see Supplementary material, Figs. S7–S8).

IR spectra of the free propyl gallate ligand in KBr displayed bands located at 3499 cm^{-1} and 3468 cm^{-1}, typical of the phenol group, and at 1688 cm^{-1} which is characteristic of stretching νC=O [29]. Aromatic stretching (1614 cm^{-1}) can be assigned to νCsp^2-H and ν 1538 cm^{-1} to the phenyl group. Asymmetric deformation in the plane (δ H Csp^2) was observed at δ 1466 cm^{-1} and at 1405 cm^{-1}. At 1301 cm^{-1} and 1248 cm^{-1}, stretches were observed regarding νC—O—C vibration, which are characteristic for propyl galate [31–33]. Three bands, at 866, 744 and 644 cm^{-1}, are originated from the angular ring deformation and angular deflections of C—H fragment [30,32] (Table 2).

After coordination of the ligand with the metals, the bands around 3468 cm^{-1}, which were assigned to hydroxyl groups, decreased in both complexes. The characteristic bands of the carbonyl group νC=O (1688 cm^{-1}) and νC—O—C (1301 and 1248 cm^{-1}) are present in the same region, without significant change, showing that the coordination did not occur by the carboxylate group [30,31]. Finally, new bands of medium intensities, located below 500 cm^{-1} are present in the spectra of the complexes, which may be related to metal–ligand vibrations [31–33], (see Supplementary material, Fig. S9–S10).

Table 2
Main bands (cm^{-1}) in the IR spectra of the PG and of complexes (**1**) and (**2**).

Band assignmentassigment	Propyl galate	(**1**)	(**2**)
νOH—Ph	3499; 3468	3481	–
νC=O	1688	1669	1704
νC—O—C	1301; 1248	1438; 1364	1431; 1393
Pt—O	–	524	–
Pt—P	–	641	–
Ru—O	–	–	578

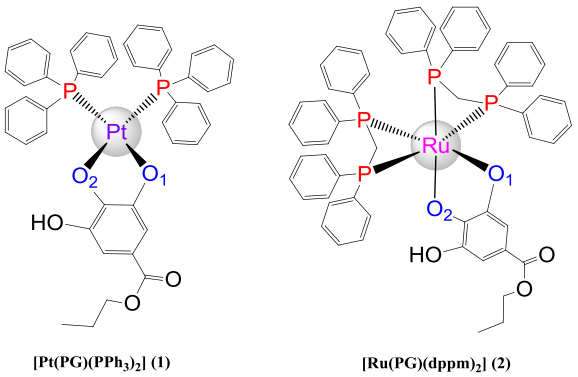

Fig. 2. Proposed structures for propyl gallate complexes.

3.1. Single-crystal X-ray diffraction results

Single-crystal X-ray diffraction measurements of complex **1** showed that it crystallizes into the space group $P\bar{1}$ triclinic with two conformers of complex **1** by asymmetric unity (Fig. 3). The main difference between conformers is the orientation of propyl chain of the gallate ligand. In conformer A, which presents a disorder in the propyl group (C91A and C92A atoms), an *anti*-orientation of the propyl chain and the free hydroxyl (O3A–H3A) of gallate ligand can be observed. The torsion angle τ_{1A} [C4A–C5A–C7A–O5A] confirms this orientation to the propyl chain (τ_{1A} = 169.0 (9)°). Conformer B presents a *syn*-orientation between the propyl chain and free hydroxyl (O3B–H3B), respectively, and the torsion angle τ_{1B} [C4B–C5B–C7B–O5B] settles this conformation (τ_{1B} = −2 (1)°).

Conformational freedom of the propyl chain of the gallate ligand is an important factor that influences the crystal packing of complex **1**. A stereographic view along (100) the plane shows the formation of columns of the conformers, which change in parallel (see Supplementary material, Fig. S11). Conformers A form columns (columns A) in which the gallate ligands are oriented pointing in the same direction of crystallographic *b*-axe, meanwhile columns of conformers B (columns B) line up the gallate ligands into the crystallographic *c*-axe. In detail, columns A are made up of two antiparallel layers in the [001] direction of conformers A related by the inversion center. In the middle of the layers, there is a formation of cavities whose voids have calculated volumes [34] approximately of 128 $Å^3$, which is related to the disposition of the disordered propyl chains of conformers A which are not linked by strong supramolecular interactions. Columns B appear as the result of stacking pairs of conformers B, which extend by translational operation along the crystallographic *a*-axis and these pairs of conformers B are related by the inversion center. Stacking conformer B molecules causes the molecules to be closer and they do not present any disorder. These pairs are united by C—H···π interactions, which are responsible for the crystal network stabilization [35]. Moreover, non-classic hydrogen bonds of C—H···O type are largely responsible by the linkage between conformers of complex **1** and, therefore the assembly between the columns. C24A–H24A···O3B (distance of 2.416(5) Å and angle of 139.81(71)° with C24A···O3B separation of 3.183(11) Å. Symmetry code: *x*, *y*, *z*) and C34B–H34B···O4A (distance of 2.658(9) Å and angle of 159.11(75)° with C34B···O4A separation of 3.542(15) Å. Symmetry code: 1 − *x*, −*y*, 1 − *z*) are the most important. The first one occurs between the free hydroxyl of the gallate ligand of conformers A and one of carbon atoms in *para*-position of tri-phenyl

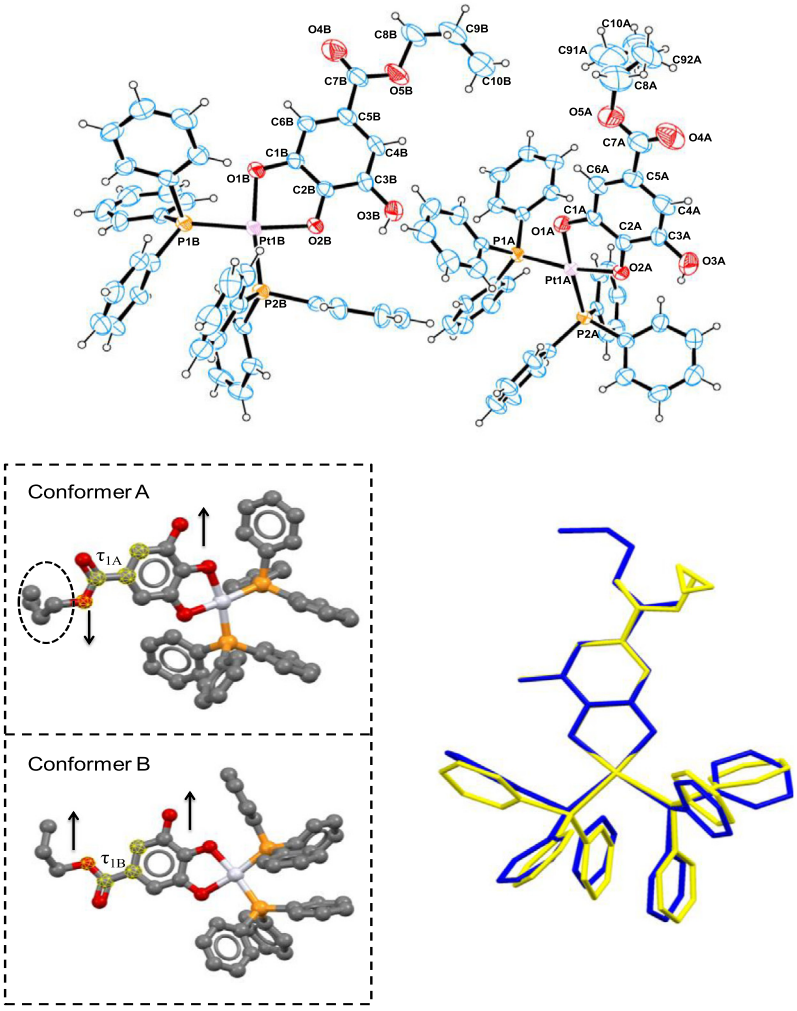

Fig. 3. ORTEP view of asymmetry unity of complex **1** with the thermal ellipsoids at the 50% probability level (Up). Overlay of molecular structures (down) for conformers A (yellow) and conformers B (blue). The torsion angle τ_1 [C4–C5–C7–O5] for both conformers is highlighted. The disorder of the propyl chain (C91A and C92A atoms) for conformers A is too highlighted by the dashed circle. (Color online.)

Table 3
IC_{50} and selectivity indexes values (μM) obtained for the propyl gallate and for complexes (**1**) and (**2**).

Tumor cell lines	PG	1	2	Cisplatin	IS1	IS2
U251MG	228.9 ± 27.3	>500	17.1 ± 0.2	9.6 ± 0.8	1.8	8.1
A549	320.1 ± 22.3	>500	36.5 ± 0.9	21.5 ± 0.6	0.8	3.6
MCF-7	236.4 ± 25.3	>500	8.5 ± 4.2	76.8 ± 4.8	3.5	1.0
HepG2	438.8 ± 21.4	>500	11.6 ± 5.3	38.5 ± 1.5	2.6	2.0
CCD-1059Sk	NT	NT	30.1 ± 3.8	77.7 ± 8.2	–	–

NT: not tested.
IS = IC_{50}CCD-1029Sk/IC_{50} (cell lines) IS1 = [Ru(GP)(dppm)$_2$] and IS2 = cisplatin.

phosphine ligand of conformers B. The second one occurs between the carbonyl oxygen of the ester group of gallate ligand on conformer A and other *para*-carbon atom of triphenylphosphine ligand on conformer B, respectively.

3.2. Biological experiments

Cytotoxic potential of propyl gallate complexes **1** and **2** were evaluated against several tumor cell lines derived from human cancers. The results showed that complex **2** is more active when compared to the free propyl gallate (Table 3). Cytotoxic activity of **2** on MCF-7 and on HepG2 is better than cisplatin, a powerful cytotoxic compound widely used in chemotherapy and used in this study as the positive control. These findings are very important considering that the mortality rate of hepatocellular carcinoma (HCC) and breast cancer are still high. HCC represents the second and most common cause of death from cancer worldwide [36] and breast cancer is responsible for about 37,000 deaths each year among women in Latin America [37].

3.2.1. BSA-binding experiments

Albumin is the most abundant protein in plasma, thus its interaction with propyl galate and complexes **1**–**2** was evaluated. These compounds bind to this protein and may lead to a reduction or

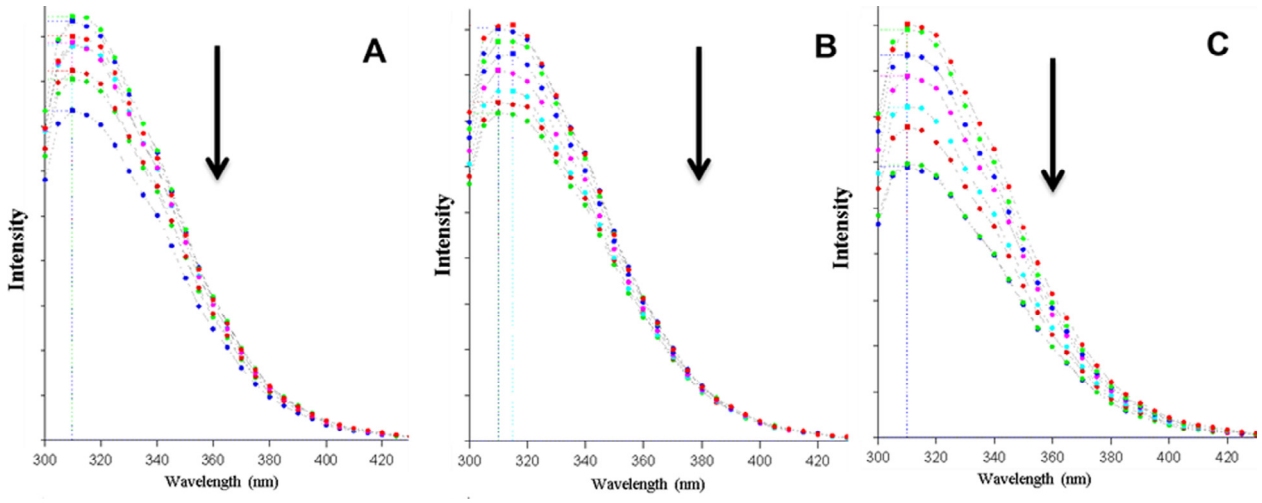

Fig. 4. Fluorescence quenching spectra of BSA with different concentrations of complex (A) Propyl gallate, (B) [Pt(PG)(PPh_3)$_2$] (C) [Ru(PG)(dppm)$_2$], with the excitation wavelength at 280 nm at 310 K in trizma buffer pH 7.4.

Table 4
Stern–Volmer quenching constant (K_{sv}, L mol^{-1}), biomolecular quenching rate constant (K_q, L mol^{-1} s^{-1}), binding constant (K_b, M^{-1}), the number of binding sites (n), ΔG (kJ·mol^{-1}), ΔH (kJ·mol^{-1}) and ΔS (J·mol^{-1} K) values for the complex-BSA system at different temperatures.

	Temp.	K_{sv} (10^4)	K_q (10^{12})	K_b (10^5)	N	ΔG	ΔH	ΔS
1	298	2.46 ± 0.10	4.00 ± 0.17	3.20 ± 0.03	1.00 ± 0.25	−31.40	−77.85	−261.30
	310	2.40 ± 0.16	3.85 ± 0.27	10.80 ± 0.60	1.50 ± 0.16	−41.70		
2	298	5.80 ± 0.15	9.35 ± 0.25	0.30 ± 0.02	0.93 ± 0.07	−25.50	−159.10	−533.73
	310	5.00 ± 0.13	8.00 ± 0.20	3.60 ± 0.15	1.17 ± 0.04	−33.00		
PG	298	2.32 ± 0.20	3.75 ± 0.03	0.20 ± 0.03	0.98 ± 0.11	−24.40	−119.80	−402.05
	310	1.70 ± 0.12	2.75 ± 0.02	1.30 ± 0.08	2.35 ± 0.16	−54.20		

enhancement of their biological properties because it presents the ability to transport drugs and nutrients through the organism [38]. The interaction of the novel complexes and propyl gallate with BSA was studied by fluorescence quenching experiments. Quenching can occur by different mechanisms, usually classified as either dynamic or static quenching, which can be distinguished by their differing dependence on temperature and viscosity, or preferably by lifetime measurements [39]. Higher temperatures result in faster diffusion and hence a larger degree of collisional quenching. Higher temperatures also result in the dissociation of weakly bound complexes and hence lead to less static quenching. As shown in Fig. 4, the BSA showed strong fluorescence emission, while the complexes displayed almost no intrinsic fluorescence under the experimental conditions used for the measurements.

The experiments were carried out in triplicate and analyzed using the classical Stern–Volmer equation: $F_0/F = 1 + K_q\tau_o[Q] = 1 + K_{sv}[Q]$, where F_0 and F are the fluorescence intensities in the absence and presence of the quencher, respectively, [Q] is the quencher concentration and K_{sv} Stern–Volmer quenching constant, which can be written as $K_q = K_{sv}/\tau_o$ where K_q is the biomolecular quenching rate constant and τ_o is the average lifetime of the fluorophore in the absence of the quencher (6.2×10^{-9} s) [40].

These results show that K_{SV} for complexes were inversely related to the increase in temperature, indicating that the probable quenching mechanism reaction is initiated by compound formation rather than by static collision. This confirms that the values of K_q in Table 4 were in the range of 3.85×10^{12}–9.35×10^{12} mol L^{-1} for all reactions of compounds–BSA, which are far higher than 2.0×10^{10} mol·L^{-1}, the maximum possible value for dynamic quenching [41]. Consequently, the probable fluorescence quenching mechanism operating on compounds–BSA binding reactions should follow a static quenching process.

The binding constant (K_b) and number of complexes bound to BSA (n) were determined by plotting the double log graph of the fluorescence data using: $\log [(F_0 - F)/F] = \log K_b + n\log[Q]$. The number of binding sites between BSA and galato complexes is approximately equal to 1, indicating that there is only one binding site in the BSA for each complex. Furthermore, the interaction constant (K_b) for all complexes is between 0.30×10^5 and 10.80×10^5 M^{-1}, which is the same range reported for Ru [38], Ni [39] and Zn [42] complexes, showing hydrophobic interactions with BSA.

In order to identify the type of interaction force acts between the complexes and BSA, thermodynamic parameters, such as free energy changes (ΔG), enthalpy changes (ΔH) and entropy changes (ΔS) of the interactions were calculated from the following equations: $\ln (K_2/K_1) = [(1/T_1) - (1/T_2)]\Delta H/R$ and $\Delta G = -RT\,\mathrm{Ln}K = \Delta H - T\Delta S$, K_1 and K_2 are the binding constants at temperatures T_1 and T_2, respectively, and R is the gas constant. From the thermodynamic standpoint, $\Delta H > 0$ and $\Delta S > 0$ imply a hydrophobic interaction; $\Delta H < 0$ and $\Delta S < 0$ reflects van der Waals force or hydrogen bond formation; and $\Delta H < 0$ and $\Delta S > 0$ suggests an electrostatic force.

As observed in Table 4, the negative ΔH and ΔS values for compounds **1**, **2** and free **PG** reveal the predominance of van der Waals force or hydrogen bond formation of these compounds with BSA. This behavior is similar to those reported for cis-bis (N-benzoyl-N′,N′-dibenzylthioureido)platinum(II) complex and BSA [43]. Furthermore, the negative ΔG values reveal that the interaction process is spontaneous.

Table 5
IC_{50} values (μM) to scavenge DPPH free radicals depending on the time.

t (min)	GA	PG	Pt
3	10.18 ± 0.37	13.21 ± 0.88	25.84 ± 1.13
9	9.71 ± 0.36	12.65 ± 0.55	24.93 ± 0.88
20	9.11 ± 0.35	12.00 ± 0.15	24.36 ± 0.26
30	8.82 ± 0.27	11.40 ± 0.26	23.54 ± 0.16

Table 6
Percentage of consumption by DPPH concentration after 30 min of incubation.

μM	AG	PG	Pt
200	90.86 ± 0.07	87.85 ± 0.25	73.64 ± 0.07
100	89.96 ± 0.61	88.61 ± 1.45	71.42 ± 0.25
50	90.11 ± 0.07	87.05 ± 0.12	64.90 ± 1.00
25	88.96 ± 0.18	82.48 ± 1.20	39.11 ± 0.45
12.50	68.70 ± 1.95	54.95 ± 2.02	21.56 ± 0.20
6.25	43.45 ± 1.62	34.01 ± 0.80	10.17 ± 0.90
3.12	27.34 ± 1.40	22.27 ± 1.45	3.54 ± 0.80
1.56	22.37 ± 2.42	17.16 ± 1.90	4.47 ± 0.25

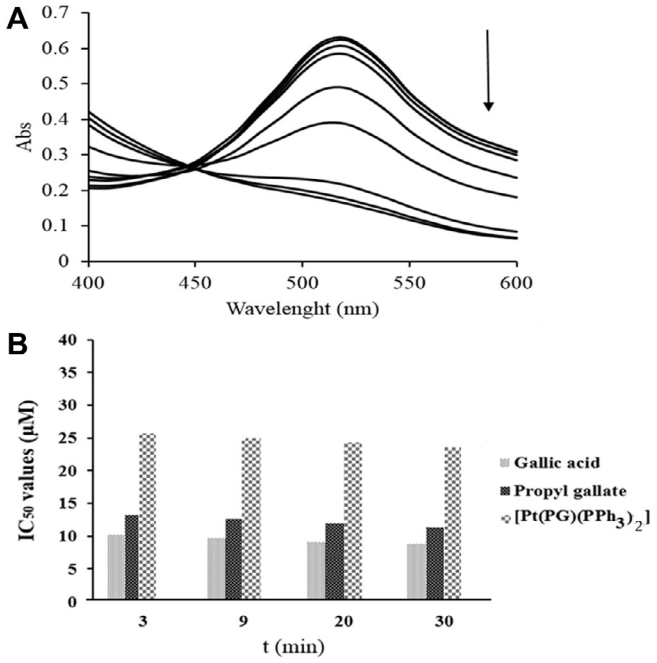

Fig. 5. (a) Absorption spectrum of DPPH with different concentrations of complex $[Pt(PG)(PPh_3)_2]$ after 30 min of incubation (b) graphic of IC_{50} values found for scavenge DPPH free radicals depending on the time.

3.2.2. Determination of free radical scavenging activity through DPPH assay

The percentage radical scavenging activity by the different complexes was determined against DPPH. As expected, the complex containing the PG coordinated showed antioxidant activity, as well as the free PG and the free GA. Regression equations to derive the IC_{50} values (concentration of compounds required to scavenge 50% DPPH free radicals) show that the reduction of DPPH decreases over time (Tables 5, 6 and Fig. 5), and in the range studied concentration (0–200 μM), it was observed that only $[Pt(PG)(PPh_3)_2]$ complex has an inhibitory effect against free radicals, whereas $[Ru(PG)(dppm)_2]$ was not active (IC_{50} > 200 μM).

To evaluate the percentage of consumption by DPPH concentration after 30 min, it can be observed (see Table 6) that the gallic acid and propyl gallate present a majority consumption of species (≈90%) in the concentration 200 μM, whereas for $[Pt(PG)(PPh_3)_2]$ at the same concentration only 70% of the species was consumed. With the decrease of the concentration of the compound, it was observed that the consumption of the free radical DPPH is more efficient for the free PG than for the complexes containing this ligand, corresponding to the same behavior observed for the IC_{50}. Interestingly, the antioxidant activity presented by $[Pt(PG)(PPh_3)_2]$ is better than that one shown by the conventional antioxidant obtained from the diet, ascorbic acid (IC_{50} = 39 μM), which is considered extremely important in the elimination of free radicals and commonly used as antioxidant food additives [44].

3.2.3. Circular dichroism experiments

Circular dichroism (CD) technique is very sensitive for diagnosing changes in the secondary structure of DNA resulting from DNA interactions with small molecules. A typical CD spectrum of CT DNA shows a maximum at 275 nm, because of the base stacking, and a minimum at 248 nm, which is attributed to the right-handed helicity of the molecule, characteristic of its B conformation. Fig. 6 shows the spectra of both complexes evaluated with CT-DNA solutions at different ratios, as well as the CD spectrum of DNA alone. Both complexes did not produce significant changes in the elipticity values for both bands, indicating that the free ligand and respective complexes cannot modify the DNA secondary structure, different behavior than reported for cisplatin and other platinum complexes [45].

4. Conclusions

Two novel propyl galate complexes of platinum and ruthenium were synthesized and characterized by a combination of NMR, UV–Vis, IR techniques. Moreover, the $[Pt(PG)(PPh_3)_2]$ complex was

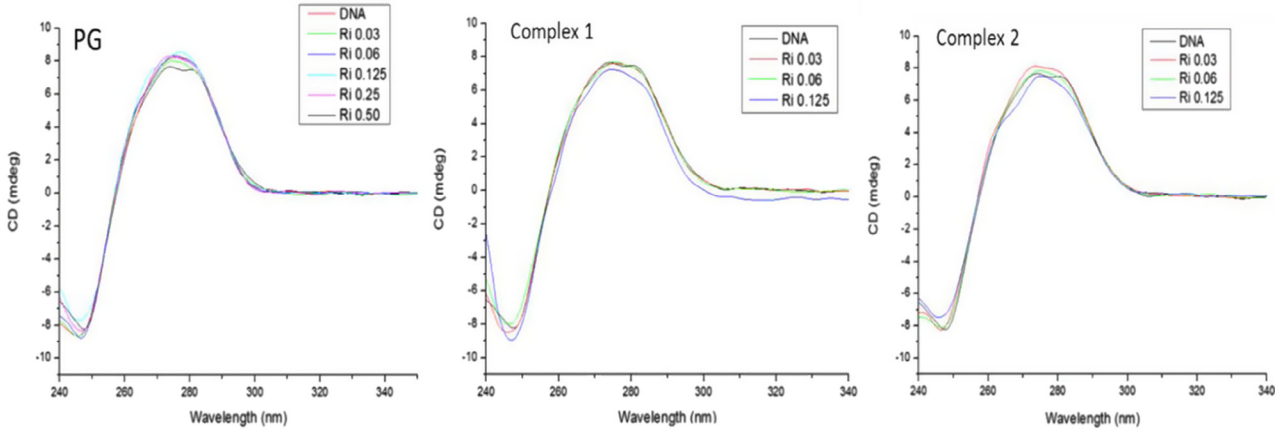

Fig. 6. Circular dichroism (CD) spectra of CT DNA incubated 18 h with propyl gallate, Pt and Ru-propyl gallate complexes at different [complex]/[DNA] ratios at 37 °C.

characterized by X-ray diffraction technique. The evaluation of antitumor activity of the complexes demonstrated that the [Ru(PG)(dppm)$_2$] complex is more potent than the free propyl gallate and the cisplatin, against the MCF-7 (breast carcinoma) and HepG2 (hepatocellular carcinoma) tumor cells. The thermodynamic parameters of the complex/BSA binding indicate a spontaneous interaction between these two species and the presence of van der Waals force or hydrogen bond formation between them. Consequently, the probable fluorescence quenching mechanism operating on the propyl gallate compounds–BSA binding reactions can be a static quenching process. It was observed that only [Pt(PG)(PPh$_3$)$_2$] complex has an inhibitory effect against free radicals, whereas the [Ru(PG)(dppm)$_2$] complex is not active.

Acknowledgements

This study received support from CNPq, FAPESP, FAPEMIG and CAPES. J.C.T. would like to thank FAPESP for a PhD fellowship (grant numbers 2013/07581-9).

Appendix A. Supplementary data

CCDC 1420349 contains the supplementary crystallographic data for (**1**). These data can be obtained free of charge via http://dx.doi.org/10.1016/j.poly.2017.03.055, or from the Cambridge Crystallographic Data Centre, 12 Union Road, Cambridge CB2 1EZ, UK; fax: (+44) 1223-336-033; or e-mail: deposit@ccdc.cam.ac.uk. Supplementary data associated with this article can be found, in the online version, at http://dx.doi.org/10.1016/j.poly.2017.03.055.

References

[1] D. Wang, S.J. Lippard, Nat. Rev. Drug Discov. 4 (2005) 307.
[2] A.P.S. Fontes, E.T. César, H. Beraldo, Cadernos Temáticos de Química Nova na Escola 6 (2005) 13.
[3] B.C. Baguley, A brief History of Cancer Chemotherapy. Anticancer Drug Develop, Academic Press, 2002, p. 397, Cap.1.
[4] A. Bergamo, C. Gaiddon, J.H.M. Schellens, J.H. Beijnen, G. Sava, J. Inorg. Biochem. 106 (2012) 90.
[5] C. Billecke, S. Finniss, L. Tahash, C. Miller, T. Mikkelsen, N.P. Farrel, O. Bogler, Neuro-oncology 8 (2006) 215.
[6] N.J. Wheate, J.G. Collins, Coord. Chem. Rev. 241 (2003) 133.
[7] M.I. Webb, C.J. Walsby, Dalton Trans. 40 (2011) 1322.
[8] Q.A. De Paula, R.W. Franco, M.B. Ribeiro, J. Ellena, E.E. Castellano, O.R. Nascimento, A.A. Batista, J. Mol. Struct. 891 (2008) 64.
[9] C.X. Zhang, S.J. Lippard, Curr. Opin. Chem. Biol. 7 (2003) 481.
[10] J. Zhang, Q. Yu, Q. Li, L. Yang, L. Chen, Y. Zhou, J. Liu, J. Inorg. Biochem. 134 (2014) 1.
[11] S. Kumar, S. Pandey, A.K. Pandey, Biomed Res Int. 2014 (2014), Article ID 495154.
[12] C. Locatelli, F. Branco, Eur. J. Med. Chem. 60 (2013) 233.
[13] H. Ching, Food and Chem. Toxicol. 49 (2011) 494.
[14] S.M. Fiuza, C. Gomes, L.J. Teixeira, M.T. Girão da Cruz, M.N. Cordeiro, N. Milhazes, F. Borges, M.P. Marques, Bioorg. Med. Chem. 12 (2004) 3581.
[15] K. Cormier, R.D. Curry, M.P. Betsch, J.A. Goguen, C.M. Vogels, A. Decken, A. Turcotte, S.A. Westcott, J. Heterocyclic Chem. (2015), http://dx.doi.org/10.1002/jhet.2490 (in press).
[16] S.J. Glynn, K.J. Gaffney, M.A. Sainz, S.G. Louie, N.A. Petasis, Org. Biomol. Chem. (2015), http://dx.doi.org/10.1039/C4OB02512A (in press).
[17] H. Jacobi, B. Eicke, I. Witte, Free Radical Biol. Medicine 24 (1998) 972.
[18] Enraf-Nonius, COLLECT. Nonius BV, Delft, The Netherlands 1997–2000.
[19] Z. Otwinowski, W. Minor, 1997. HKL Denzo and Scalepack. Methods in Enzymology 276, edited by C.W. Carter, Jr., R.M. Sweet pp. 307–326, New York: Academic Press.
[20] G.M.A. Sheldrick, Acta Crystallogr. Sect. A Found. Crystallogr. 64 (2008) 112.
[21] P. Coppens, L. Leiserowitz, D. Rabinovich, Acta Crystallogr. 18 (1965) 1035.
[22] L.J. Farrugia, J. Appl. Crystallogr. 32 (1999) 837.
[23] L.J. Farrugia, J. Appl. Crystallogr. 30 (1997) 527.
[24] C.F. Macrae, I.J. Bruno, J.A. Chisholm, P.R. Edgington, P. McCabe, E. Pidcock, L. Rodriguez-Monge, R. Taylor, J. van de Streek, P.A. Wood, J. App. Crystallogr. 41 (2008) 466.
[25] J.X. McDermott, J.F. White, G.M. Whitesides, J. Am. Chem. Soc. 98 (1976) 6521.
[26] B.P. Sullivan, T.J. Meyer, Inorg. Chem. 21 (1982) 1037.
[27] L. Colina-Vegas, W. Villarreal, M. Navarro, C.R. de Oliveira, A.E. Graminha, P.I.S. Maia, V.M. Deflon, A.G. Ferreira, M.R. Cominetti, A.A. Batista, J. Inorg. Biochem. 153 (2015) 150.
[28] W. Brand-Williams, M.E. Cuvelier, C. Berset, Lebenson Wiss. Technol. 28 (1995) 25.
[29] B. Badhani, N. Sharma, R. Kakkar, RSC Adv. 5 (2015) 27540.
[30] N.R. Perron, J.L. Brumaghim, Cell Biochem Biophys. 53 (2009) 75.
[31] A.D. Wilson, D.T. Lewis, Analyst. 88 (1963) 585.
[32] M.I.F. Barbosa, R.S. Corrêa, L.V. Pozzi, É.O. Lopes, F.R. Pavan, C.Q.F. Leite, J. Ellena, S.P. Machado, G.V. Poelhsitz, A.A. Batista, Polyhedron 85 (2015) 376.
[33] M.I.F. Barbosa, R.S. Corrêa, K.M. de Oliveira, C. Rodrigues, J. Ellena, O.R. Nascimento, V.P. Rocha, F.R. Nonato, T.S. Macedo, J.M. Barbosa-Filho, M.B. Soares, A.A. Batista, J. Inorg. Biochem. 139 (2014) 33–39.
[34] K. Nakamoto, Infrared and Raman Spectra of Inorganic and Coordination Compounds, 5ª ed. Parte B., Wiley-Interscience, New York, 1997, p. 384.
[35] A.L. Spek, J. Appl. Crystallogr. 36 (2003) 7.
[36] G.G.R. Desiraju, T. Steiner, The Weak Hydrogen Bond: In Structural Chemistry and Biology, Oxford University Press on Demand, 2001.
[37] L.A. Torre, F. Bray, R.L. Siegel, J. Ferlay, J. Lortet-Tieulent, A. Jemal, A Cancer J. for Clinicians 65 (2015) 87.
[38] D.C. Allred, J.M. Harvey, M. Berardo, G.M. Clark, Modern Pathol. J. U. S. Canadian Acad. Pathol. 11 (1998) 155–168.
[39] F.R. Lima, S.A. Kahn, R.C. Soletti, Biochim. Biophys. Acta 2 (2012) 338.
[40] F. Xue, C.-Z. Xie, Y.-W. Zhang, Z. Qiao, X. Qiao, J.-Y. Xu, S.-P. Yan, J. Inorg. Biochem. 115 (2012) 78.
[41] E. Gratton, N. Silva, G. Mei, N. Rosato, I. Savini, A. Finazzi-Agro, Int. J. Quantum Chem. 42 (1992) 1479.
[42] X. Zhao, R. Liu, Z. Chi, Y. Teng, P. Qin, J. Phys. Chem. 114 (2010) 5625.
[43] M. Ganeshpandian, R. Loganathan, E. Suresh, A. Riyasdeen, M. Abdulkad, M. Palaniandavar, Dalton Trans. 43 (2014) 1203.
[44] R.S. Correa, K.M. Oliveira, H. Pérez, A.M. Plutín, R. Ramos, R. Mocelo, E.E. Castellano, A.A. Batista, Arab. J. Chem. (2015), http://dx.doi.org/10.1016/j.arabjc.2015.10.006 (in press).
[45] W. Villarreal, L. Colina-Vegas, C.R. de Oliveira, J.C. Tenorio, J. Ellena, F.C. Gozzo, M.R. Cominetti, A.G. Ferreira, M.A.B. Ferreira, M. Navarro, A.A. Batista, Inorg. Chem. 54 (2015) 11709.